Whole-tree mesophyll conductance reconciles isotopic and gas-exchange estimates of water-use efficiency

Teresa E. Gimeno[1, 2*], Courtney E. Campany[3], John E. Drake[4], Craig V. M. Barton[5], Mark G. Tjoelker[5], Nerea Ubierna[6] and John D. Marshall[7]

[1]Basque Centre for Climate Change (BC3), 48940, Leioa, Spain
[2]IKERBASQUE, Basque Foundation for Science, 48008, Bilbao, Spain
[3]Department of Biology, Shepherd University, Shepherdstown, WV 25443, USA
[4]Forest and Natural Resources Management, SUNY-ESF, Syracuse, NY 132110, USA
[5]Hawkesbury Institute for the Environment, Western Sydney University, Penrith NSW 2751, Australia
[6]Research School of Biology, The Australian National University, Acton ACT 2601, Australia
[7]Department of Forest Ecology and Management, Swedish University of Agricultural Sciences (SLU), Skogsmarksgränd 17, 907 36, Umeå, Sweden

Accepted for publication in *New Phytologist* on 7th November 2020

* Corresponding author:
Teresa E. Gimeno
E-mail: teresa.gimeno@bc3research.org

SUMMARY

- Photosynthetic water-use efficiency (WUE) describes the link between terrestrial carbon and water cycles. Estimates of intrinsic WUE (iWUE) from gas-exchange and carbon isotopic composition ($\delta^{13}C$) differ due to an internal conductance in the leaf mesophyll (g_m) that is variable and seldom computed.
- We present the first direct estimates of whole-tree g_m, together with iWUE from whole-tree gas-exchange and $\delta^{13}C$ of the phloem ($\delta^{13}C_{ph}$). We measured gas-exchange, online ^{13}C-discrimination and $\delta^{13}C_{ph}$ monthly throughout spring, summer and autumn in *Eucalyptus tereticornis* grown in large whole-tree chambers. Six trees were grown at ambient temperatures and six at a 3°C warmer air temperature; a late-summer drought was also imposed.
- Drought reduced whole-tree g_m. Warming had few direct effects, but amplified drought-induced reductions in whole-tree g_m. Whole-tree g_m was similar to leaf g_m for these same trees. iWUE estimates from $\delta^{13}C_{ph}$ agreed with iWUE from gas-exchange, but only after incorporating g_m. $\delta^{13}C_{ph}$ was also correlated with whole-tree ^{13}C-discrimination, but offset by -2.5±0.7‰, presumably due to post-photosynthetic fractionations.
- We conclude that $\delta^{13}C_{ph}$ is a good proxy for whole-tree iWUE, with the caveats that post-photosynthetic fractionations and intrinsic variability of g_m should be incorporated to provide reliable estimates of this trait in response to abiotic stress.

KEYWORDS

Carbon stable isotope, drought, *Eucalyptus*, phloem, photosynthesis, respiration, warming, whole-tree chamber.

INTRODUCTION

Water use efficiency (WUE), the ratio of carbon uptake per unit water loss, is a fundamental tradeoff governing vegetation functioning and the global cycles of carbon, water and energy (Eamus, 1991; Keenan *et al.*, 2013). Ecosystem models rely on measurements of WUE to validate their predictions of vegetation-atmospheric feedbacks (Rogers *et al.*, 2017). WUE is a complex trait (Flexas *et al.*, 2016); it varies among and within species (Aranda *et al.*, 2012; Shrestha *et al.*, 2019) and it is influenced by morphological characteristics and physiological processes operating at different scales, from the leaf ultrastructure (Tomas *et al.*, 2013; Veromann-Jurgenson *et al.*, 2017; Shrestha *et al.*, 2019) to the whole canopy (Duursma & Marshall, 2006; Campany *et al.*, 2016).

Originally, WUE was defined as the ratio of biomass gain to water loss (e.g., Hsiao & Acevedo, 1974). Methods to estimate WUE differ in spatial and temporal scales: from individual leaves up to entire ecosystems; and from instantaneous measurements to estimates integrated over growing seasons (Medlyn *et al.*, 2017; Guerrieri *et al.*, 2019). For individual plants or leaves, instantaneous WUE is calculated from gas-exchange measurements (von Caemmerer & Farquhar, 1981), whereas time-integrated measurements of WUE are often inferred from C stable isotopic composition ($\delta^{13}C$) of plant material (Farquhar *et al.*, 1989). For example, $\delta^{13}C$ of leaves or tree-ring cellulose are used to derive WUE integrated over the ontogeny of a certain organ or tissue (Marshall & Monserud, 1996; Kohn, 2010), whereas $\delta^{13}C$ from the phloem or leaf sugars reflects WUE integrated over a smaller time-window of 1-3 days (Keitel *et al.*, 2006; Tarin *et al.*, 2020). At the ecosystem scale, WUE is calculated as the ratio of gross primary productivity to evapotranspiration, derived from eddy covariance flux measurements (Keenan *et al.*, 2013; Medlyn *et al.*, 2017). Additionally, measurements of $\delta^{13}C$ of atmospheric CO_2 reveal changes in WUE across larger spatial and temporal scales (Fung *et al.*, 1997), in response to drought episodes (Peters *et al.*, 2018), increasing atmospheric [CO_2] (Bowling *et al.*, 2014) or water vapor pressure deficit (Raczka *et al.*, 2016). However, these methods often yield disparate WUE estimates, even when compared within plant functional types and similar scales (Medlyn *et al.*, 2017; Tarin *et al.*, 2020).

One problem that arises when comparing WUE estimates is that they differ in the [CO_2] and [H_2O] gradients incorporated into their calculations (Seibt *et al.*, 2008; Barbour *et al.*, 2016).

A common proxy of WUE is intrinsic water-use efficiency (iWUE), the ratio of net photosynthesis (A_{net}) to stomatal conductance to water vapor (g_s, usually in mol H_2O m^{-2} s^{-1}), but the pathways into and out of the leaf for CO_2 and water reflected in iWUE are not exactly the same. For a given vapor pressure deficit, the rate of water loss depends on boundary layer and stomatal conductances, whereas the rate of CO_2 uptake additionally depends on the rate of carboxylation and CO_2 mesophyll conductance (g_m, usually in mol CO_2 m^{-2} s^{-1}), the pathway from the substomatal cavity to the site of carboxylation (Evans *et al.*, 2009). In C_3 species, the magnitude of g_m is comparable to that of g_s; thus both conductances limit photosynthesis and WUE (Flexas *et al.*, 2012).

The influence of g_m on WUE is revealed when comparing iWUE estimates from gas-exchange and $\delta^{13}C$ methods (Fung *et al.*, 1997), which differ in the $[CO_2]$ gradient implicit in their calculations (Pons *et al.*, 2009). iWUE calculated from measurements of gas-exchange reflects the $[CO_2]$ gradient between the atmosphere and the substomatal cavity, which depends on boundary and stomatal (g_s) conductances; whereas, iWUE from $\delta^{13}C$ of plant material is proportional to the $[CO_2]$ gradient between the atmosphere and the site of carboxylation, which additionally depends on g_m (Warren & Dreyer, 2006; Michelot *et al.*, 2011). Many studies comparing iWUE estimates neglect g_m limitations to photosynthesis (Medlyn *et al.*, 2017; Guerrieri *et al.*, 2019; Tarin *et al.*, 2020; although see: Michelot *et al.*, 2011; Vernay *et al.*, 2020). Fortunately, measurements of g_m are becoming increasingly available for many species under varying climatic conditions, owing to methodological advances (Pons *et al.*, 2009), but more importantly due to the recognition of the crucial role of g_m in regulating vegetation carbon-water tradeoffs (Flexas *et al.*, 2012; Sun *et al.*, 2014; Raczka *et al.*, 2016).

This recognition has led to further studies of how g_m varies among plant functional types and with environmental and climatic drivers. For example, at the leaf level, g_m increases with temperature in some species (Warren & Dreyer, 2006; Warren, 2008a; Evans & von Caemmerer, 2013; von Caemmerer & Evans, 2015; Shrestha *et al.*, 2019). Other studies have found no temperature effects on g_m (Dillaway & Kruger, 2010) or even a decrease with temperature (Qiu *et al.*, 2017). Importantly, the temperature response of g_m may differ depending on the temperature range (Silim *et al.*, 2010). In contrast, the effects of water stress appear to be more consistent: g_m usually decreases with water stress, in a coordinated manner with g_s, although the effect size varies among species and growth conditions (Grassi & Magnani, 2005; Limousin *et al.*, 2010; Flexas *et al.*, 2012; Cano *et al.*, 2013). Besides temperature and water availability, leaf-level g_m may vary

with multiple external and endogenous factors including leaf age, light, CO_2 or nitrogen content (see Niinemets *et al.*, 2009 for a review). Thus, at the scale of entire tree crowns, variation in light environment or leaf traits may complicate efforts to quantify g_m and its role in WUE; for example, nitrogen content and shading co-vary within the crown and with leaf age (Duursma & Marshall, 2006). This covariation within the crown makes it difficult to predict ecosystem-scale or whole-tree g_m from individual leaf-level measurements (Schaufele *et al.*, 2011). Nonetheless, estimates of canopy, or at least whole-tree g_m would enable a direct comparison of WUE measurements across methods and to scale up from leaves.

Canopy g_m can be calculated from ecosystem flux measurements, combined with estimates of average electron transport rate and leaf area distribution (Keenan *et al.*, 2010a). Indeed, incorporating mesophyll diffusion limitations can improve predictions of drought-induced reductions to photosynthesis at the ecosystem level (Keenan *et al.*, 2010b). However, there are some caveats to this approach: first, a relatively detailed characterization of the canopy profile is required, together with several assumptions regarding photosynthetic and respiratory responses to light and temperature. Furthermore, this approach is limited to sites with eddy covariance flux towers.

The $\delta^{13}C$ of plant material provides a time-integrated proxy of WUE, with leaf $\delta^{13}C$ as the most widely collected data (Cornwell *et al.*, 2017; Medlyn *et al.*, 2017). Leaves are easy to sample and process and isotopic analyses of plant material have become relatively quick and inexpensive. However, the vast majority of leaf measurements neglect within-crown variability, although leaf $\delta^{13}C$ is sensitive to light availability and, in evergreens, to leaf age (Ehleringer *et al.*, 1986; Duursma & Marshall, 2006; Aranda *et al.*, 2007; Gimeno *et al.*, 2012; Campany *et al.*, 2016). An alternative to leaf $\delta^{13}C$ is the $\delta^{13}C$ of phloem contents ($\delta^{13}C_{ph}$), which may serve as an independent estimate of iWUE (Pate *et al.*, 1998; Cernusak *et al.*, 2003; Merchant *et al.*, 2010). The $\delta^{13}C$ of phloem contents, when sampled below the crown on the main stem, should integrate ^{13}C-discrimination of recent photosynthate at the whole-tree scale, including all leaf layers and ages. In addition, $\delta^{13}C_{ph}$ should be representative of the most recent physiological activity, because phloem contents are completely replaced at regular intervals. (Barbour *et al.*, 2007; Ubierna & Marshall, 2011). In any case, we expect iWUE estimated from $\delta^{13}C$ of plant material, either from leaves or phloem contents, to be larger than iWUE from gas-exchange, because the former is

sensitive to g_m as well as to post-photosynthetic fractionation (Farquhar *et al.*, 1989; Gessler *et al.*, 2014).

Here, we measured whole-tree *in situ* gas and isotopic exchange, in a unique set of large, outdoor whole-tree chambers (WTCs) with trees grown under contrasting climatic conditions: experimental warming and drought. This allowed us to estimate whole-tree g_m and whole-tree iWUE from gas-exchange ($iWUE_{ge}$), spanning spring through autumn. We compared $iWUE_{ge}$ with estimates of whole-tree iWUE derived from $\delta^{13}C$ values of trunk phloem ($iWUE_{\Delta}$). We used these data to: (*i*) quantify whole-tree g_m and compare it to leaf-level g_m, (*ii*) test whether the differences between $iWUE_{ge}$ and $iWUE_{\Delta}$ can be reconciled by accounting for g_m in $iWUE_{\Delta}$ calculations and (*iii*) test whether $\delta^{13}C_{ph}$ could serve as a proxy of whole-tree iWUE. We predicted that whole-tree g_m would be comparable to leaf-level g_m, measured on the same trees, and representative of the intra-crown variability of this trait (Campany *et al.*, 2016). We also predicted that g_m would be the underlying cause of the observed discrepancies between the gas-exchange and isotope methodologies for estimating iWUE.

MATERIALS AND METHODS

Site description, experimental design and leaf area

A detailed description of the experimental design can be found in Drake *et al.*, (2016), and of the WTC functioning in Medhurst *et al.*, (2006) and Barton *et al.*, (2010). Briefly, the WTCs were located at the Hawkesbury Forest Experiment near Richmond (NSW, Australia). Each WTC consisted of a cylindrical structure topped with a cone (9 m tall, 3.25 m diameter, 53 m^3 volume) that enclosed a single tree rooted in the soil. The soil at the site was a sandy loam of alluvial origin with low-fertility (0.7% organic C, 380 and 108 mg kg^{-1}, total N and P, respectively). Roots grew inside an exclusion barrier that extended from the chamber walls down to 1 m depth into a layer of cemented manganese which restricted, but did not eliminate, root growth to deeper soil depths. In the Austral autumn, March 2013, one *Eucalyptus tereticornis* Sm. was planted in each WTC and irrigated weekly with 70 L, until September 2013, and then from October 2013, trees were watered fortnightly with half of the mean monthly rainfall for Richmond (NSW, Australia). In late summer, February 2014, a drought treatment with two levels (control and drought) was imposed by interrupting watering on half of the trees (Table S1). Soil volumetric water content (Fig. S1 a-

c) and pre-dawn leaf water potential (Fig. S1d) decreased in WTCs assigned to the drought treatment from mid-February 2014 onwards. Further details on the methodology for the monitoring of these variables and associated results can be found in Drake *et al.*, (2019b). Throughout the experiment, six WTCs tracked ambient temperature and six experienced an air temperature 3˚C warmer (Table S1). Relative humidity inside all WTCs was controlled to match that of ambient, hence vapor pressure deficit was higher in warmed than in ambient chambers (Drake *et al.*, 2016). During daylight hours, relative humidity averaged 62.5 ± 20% in the ambient and 62.4 ± 20% in the warmed treatment (Drake *et al.*, 2016). Mean [CO_2] during daylight hours was maintained at 10 μmol mol^{-1} above ambient by adding CO_2 with a controlled injection system.

Leaf area of each tree at the end of the experiment (May 2014) was calculated from destructive harvests. Throughout the experiment litterfall was collected, dried and weighed fortnightly and measurements of leaf number per branch, size and number of branches were collected at two points in time during the experiment. Individual tree leaf area at different points in time was then calculated based on allometric relationships and integrated litterfall (Barton *et al.*, 2010; Drake *et al.*, 2016; Drake *et al.*, 2019b). Our measurements commenced in spring, October 2013, when trees had reached ample crown development. At this point in time, mean (±se, n = 6 trees per temperature treatment) stem diameter (at 65 cm from the stem base) was 28.2±1.1 and 34.1±2.1 mm, tree height was 348±15.1 and 418.3±23.1 cm, and tree leaf area was 3.9±0.1 and 6.2±0.2 m^2, for ambient and warmed trees, respectively (see Drake *et al.*, 2016 for further details).

Whole-tree gas-exchange and calculation of whole-tree $iWUE_{ge}$

Whole-tree gas-exchange rates and derived variables were calculated from water and CO_2 fluxes measured with the WTC system as described in Barton *et al.*, (2010) and Drake *et al.*, (2016). Briefly, the system measured continuously all twelve chambers over 15-min cycles. The system measured the air entering and leaving the aboveground compartment, isolated from soil gas efflux by a suspended floor sealed around the base of the bole. Whole-tree photosynthesis (A_{net}) was calculated from the [CO_2] entering and leaving the WTC, the pure CO_2 added by the injector and the calculated change in CO_2 storage (if any) over the measurement cycle. Similarly, whole-tree transpiration was calculated from the water vapor entering and leaving the WTC, the change in storage and water condensed by the cooling system. All rates of gas-exchange were expressed per

unit of leaf area by dividing by the leaf area of each individual tree, estimated at different points in time (Drake *et al.*, 2016; Drake *et al.*, 2019b). One estimate of whole-tree A_{net} and transpiration was calculated for each 15-min cycle. Whole-tree stomatal conductance to water (g_s, in mol H_2O m^{-2} s^{-1}) and whole-tree [CO_2] in the substomatal cavity (C_i) were calculated according to von Caemmerer & Farquhar (1981) and assuming that in our well-ventilated WTC, with continuously operating external air-handling units, boundary layer resistance was negligible (see Methods S1 for further details). These measurements were used to calculate whole-tree intrinsic water-use efficiency as (iWUE, Fig. 1):

(Eq. 1)

$$\mathrm{iWUE_{ge}} = \frac{A_{\mathrm{net}}}{g_{\mathrm{s}}}.$$

Whole-tree isotope-exchange and calculation of whole-tree g_m

From October 2013 to April 2014, we performed six monthly campaigns (except for November 2013, Table S1) where we measured online carbon isotopic composition ($\delta^{13}C$) of the CO_2 entering and leaving the WTCs. Each campaign was performed over two consecutive sunny days (Table S1) and always over the weekend, to avoid user interference due to door opening. All twelve WTCs were measured during each campaign, with six randomly selected WTCs (three ambient and three warmed) measured each day (Table S1). A tunable diode laser absorption spectroscope (TDLAS, TGA100, Campbell Scientific, Inc., Logan, UT, USA) was deployed in the field for online measurements of $\delta^{13}C$ in air. The TDLAS was coupled to a manifold system to measure $\delta^{13}C$ of incoming and outgoing CO_2 from each WTC, after passing through a Nafion dryer. Two calibration gases, drawn from compressed air tanks of known [CO_2] (328 and 785 μmol mol^{-1}), were measured at the beginning of each sequence. Then, the incoming and outgoing gas streams of the six WTCs were measured twice during 8 min loops, for 24 h. Each line (gas stream or calibration) was measured for 20 s and the average of the last 10 s was auto-logged.

These measurements were used, following an approach conceptually similar to a "big-leaf" model (Sellers *et al.*, 1997), to calculate whole-tree observed isotope discrimination (Δ_o, Evans *et al.*, 1986) and subsequently whole-tree g_m according to Evans & von Caemmerer (2013):

(Eq. 2)

209 $$g_{\mathrm{m}} = \frac{(b - a_{\mathrm{i}} - \frac{eR_{\mathrm{d}}}{A_{\mathrm{net}} + R_{\mathrm{d}}}) \frac{A_{\mathrm{net}}}{C_{\mathrm{a}}}}{\Delta_{\mathrm{i}} - \Delta_{\mathrm{o}} - \Delta_{\mathrm{e}} - \Delta_{\mathrm{f}}}.$$

210 In Eq. 2, b, a_i and e are fractionation factors due to carboxylation (b, 29‰), diffusion through
211 water (a_i, 1.8‰) and respiration (e, 3.4‰, see Methods S1); Δ_i, Δ_e and Δ_f are the contributions to
212 fractionation of air diffusion and carboxylation (Δ_i), respiration (Δ_e) and photorespiration (Δ_f); C_a
213 is the [CO_2] surrounding the crown and R_d is daytime respiration. We used concurrent
214 measurements of A_{net}, R_d, photorespiration and their temperature sensitivity (Aspinwall *et al.*,
215 2016; Way *et al.*, 2019) to estimate Δ_i, Δ_e and Δ_f and we considered the fractionation factors to be
216 invariant with temperature for our measurement range (Evans & Von Caemmerer, 2013), see
217 Methods S1 and Fig. S2 for further details.
218
219 *Phloem contents $\delta^{13}C$ and calculation of whole-tree $iWUE_{\Delta}$*
220 The morning after each measurement day (within 1-2 h after sunrise), a tree core (~1 cm long and
221 5 mm diameter) was collected from the bole 10-15 cm below the lowest branch, at ~0.6 m above
222 the ground, from each tree in all campaigns (except from April 2014). The cores were placed in
223 glass vials with deionized water and phloem contents were allowed to exude for 24 h (Gessler *et*
224 *al.*, 2007). The solution was stored frozen until analyzed. Prior to isotopic analysis, the extracted
225 solution was dried into tin cups and carbon isotopic composition ($\delta^{13}C$) of the phloem contents
226 ($\delta^{13}C_{ph}$) was determined using isotope ratio mass spectrometry (IRMS, Delta V, Thermo Finnigan,
227 Thermo Fisher Scientific, Bremen, Germany) at the University of Sydney (NSW, Australia).
228 Isotopic composition was expressed relative to standard Vienna Pee Dee Belemnite. Values of
229 $\delta^{13}C_{ph}$ were used to estimate whole-tree discrimination (Δ_{ph}) according to (Fig. 1):
230 (Eq. 3)

231 $$\Delta_{\mathrm{ph}} = \frac{1000(\delta^{13}\mathrm{C_a} - \delta^{13}\mathrm{C_{ph}})}{1000 + \delta^{13}\mathrm{C_{ph}}},$$

232 where $\delta^{13}C_a$ is midday mean $\delta^{13}C$ of the CO_2 in the WTC air (see Methods S1 for details).
233 Measurements of Δ_{ph} were combined with theoretical models of photosynthetic
234 discrimination to solve for C_i (details bellow), which was then used to calculate whole-tree iWUE
235 (Fig. 1) as (von Caemmerer & Farquhar, 1981):
236 (Eq. 4)

$$\mathrm{iWUE} = \frac{A_{\mathrm{net}}}{g_{\mathrm{s}}} = \frac{C_{\mathrm{a}} - C_{\mathrm{i}}}{1.6},$$

The calculation of C_i depends on the theoretical model used to describe photosynthetic discrimination (Δ). The most simplified model is (Farquhar *et al.* 1989):

(Eq. 5)

$$\Delta = a_{\mathrm{s}} + \left(\bar{b} - a_{\mathrm{s}}\right)\frac{C_{\mathrm{i}}}{C_{\mathrm{a}}},$$

where a_s is the fractionation factor for gaseous diffusion (a_s, 4.4‰) and $\bar{b}$ represents effective fractionation due to carboxylation (27‰) estimated empirically (Farquhar *et al.* 1982). Solving C_i from Eq. 5, and substituting that expression of C_i into Eq. 4 results:

(Eq. 6)

$$\mathrm{iWUE}_{\Delta} = \frac{C_{\mathrm{a}}}{1.6}\frac{\bar{b} - \Delta}{\bar{b} - a},$$

where iWUE_Δ is whole-tree intrinsic water-use efficiency calculated from photosynthetic discrimination (Δ) using the simple discrimination model (Eq. 5). Here, iWUE_Δ was calculated with Δ_{ph}.

An intermediate model for discrimination (Δ_{gm}) that includes the effect of internal conductance to CO_2 diffusion on Δ is (Fig. 1, Ubierna & Farquhar 2014):

(Eq. 7)

$$\Delta_{g\mathrm{m}} = a_{\mathrm{s}} + (a_{\mathrm{i}} - a_{\mathrm{s}})\frac{C_{\mathrm{i}}}{C_{\mathrm{a}}} + (b - a_{\mathrm{i}})\frac{C_{\mathrm{c}}}{C_{\mathrm{a}}},$$

where a_i and b are the same fractionation factors as in Eq. 2 and C_c is $[CO_2]$ at the site of carboxylation, which can be substituted by $C_c = C_i - A_{net}/g_m$. As before, solving C_i from Eq. 7 and substituting that expression of C_i into Eq. 4 results in:

(Eq. 8)

$$\mathrm{iWUE}_{\Delta - g\mathrm{m}} = \frac{1}{1.6(b - a_{\mathrm{s}})}\left[C_{\mathrm{a}}(b - \Delta) + (a_{\mathrm{i}} - b)\frac{A_{\mathrm{net}}}{g_{\mathrm{m}}}\right],$$

where $\mathrm{iWUE}_{\Delta\text{-}gm}$ is whole-tree intrinsic water-use efficiency calculated from photosynthetic discrimination (Δ) using the discrimination model that accounts for the effect of g_m on Δ (Eq. 7). Here, $\mathrm{iWUE}_{\Delta\text{-}gm}$ was calculated with Δ_{ph} and whole-tree g_m estimated independently with Eq. 2 (see Methods S1 for further details). We also solved C_i from the complete photosynthetic discrimination model using the Cernusak *et al.* (2018) quadratic formulation, but we found that it did not improve predictions of C_i compared with the Δ_{gm} model (Methods S2, Table S3). A

schematic representation of our approach to calculate $iWUE_{ge}$, $iWUE_{\Delta}$ and $iWUE_{\Delta\text{-}gm}$ from gas-exchange and isotope measurements is provided in Fig. 1.

Post-photosynthetic fractionation would have an imprint on $\delta^{13}C_{ph}$ and in turn on $iWUE_{\Delta}$, but not on $iWUE_{ge}$ (Gessler *et al.*, 2008). We therefore calculated the mean (n = 6 campaigns) magnitude of post-photosynthetic fractionation (Δ_{post}) as the difference between $\delta^{13}C_{ph}$ and $\delta^{13}C$ of photosynthesis ($\delta^{13}C_{Anet}$) as:

(Eq. 9)

$$\Delta_{post} = \delta^{13}C_{Anet} - \delta^{13}C_{ph}.$$

We calculated $\delta^{13}C_{Anet}$ from mean midday $\delta^{13}C$ and $[CO_2]$ entering ($\delta^{13}C_e$ and C_e) and leaving ($\delta^{13}C_o$ and C_o) the WTC (Evans *et al.*, 1986; Methods S1):

(Eq. 10)

$$\delta^{13}C_{Anet} = \frac{\delta^{13}C_o \times C_o - \delta^{13}C_e \times C_e}{C_o - C_e}.$$

We incorporated the effect of post-photosynthetic fractionation on $iWUE_{\Delta\text{-}gm}$ (Eq. 8) by recalculating Δ_{ph} (Eq. 3) with a corrected estimate of phloem isotopic composition ($\delta^{13}C_{ph\text{-}corr} = \delta^{13}C_{ph} + \Delta_{post}$).

Statistical analyses

All statistical analyses were performed in the R environment v. 3.6.0 (R Development Core Team, 2019). Given the complex nature of the variations in g_m with the ratio of A_{net} to respiration (Busch *et al.*, 2020) and with confounding factors co-varying over daily time courses; such as temperature or light (Grassi *et al.*, 2009; Théroux-Rancourt & Gilbert, 2017); we simplified our analyses by using only whole-tree physiological parameters (g_m, A_{net}, g_s and $iWUE_{ge}$) measured at midday (10.30-13.30) and under non-limiting light availability (photosynthetic photon flux density ≥ 800 μmol m^{-2} s^{-1}). This rendered a mean of 21±2 observations per WTC and campaign. We assessed differences between temperature (ambient vs. warmed) and watering (control vs. drought) treatments and among campaigns using linear mixed models (LMMs) with temperature treatment, watering, campaign, and their interactions as fixed factors and chamber as random factor, using package 'lme4' (Bates *et al.*, 2015). The variance explained (R^2) by fixed and random factors was computed by comparing marginal (R^2_m, fixed) and conditional (R^2_c, fixed and random) R^2 (Nakagawa & Schielzeth, 2013). Prior to analyses, some variables were ln-transformed. We

analyzed the relationship between midday whole-tree g_m and air temperature (excluding trees from the drought treatment after February 2014) with generalized additive mixed models (GAMMs). We used package 'mgcv' to fit a GAMM to whole-tree g_m with air temperature inside the WTC as predictor, taking into account the random chamber-to-chamber variability and without making any *a priori* assumptions on the shape of the relationship between whole-tree g_m and temperature (Duursma *et al.*, 2014). Significant differences ($\alpha = 0.05$) between ambient and warmed trees were assessed graphically based on non-overlapping 95% confidence intervals. According to the LMMs results, neither the warming nor the drought treatment had any significant effect on the regression relationships between iWUE estimates or between $\delta^{13}C$ measurements. Hence, the effects of the warming and drought treatments were not included in the correlation analyses. We assessed the regression relationships between: $\delta^{13}C_{ph}$ and $\delta^{13}C_{Anet}$ and $\delta^{13}C_{ph}$, and between independent estimates of iWUE ($iWUE_{ge}$ with $iWUE_{\Delta}$ and with $iWUE_{\Delta\text{-}gm}$,) with random intercept LMMs, including chamber as a random factor.

RESULTS

Whole-tree gas-exchange and g_m *across campaigns, temperature and drought treatments*

Physiological parameters (g_s, A_{net} and $iWUE_{ge}$) varied among campaigns and between experimental treatments (Table S2, Fig. S3), providing a source of variation used in the method comparisons. Neither warming nor drought had any significant direct or indirect effect on $iWUE_{ge}$. However, warming decreased A_{net} and the campaign × warming interaction was significant for A_{net} and g_s: warming-induced reductions in g_s and A_{net} were most pronounced in summer (Fig. S3). The drought treatment significantly reduced A_{net} and g_s (Table S2) and this reduction varied among campaigns and within temperature treatments ($P = 0.003$ for the three-way interaction): the reduction under drought was more pronounced in the summer and in warmed trees (Fig. S3).

Whole-tree g_m varied among campaigns (Fig. 2, Table S2): whole-tree g_m was higher in spring (October 2013) than in summer (December 2013). Similar to what Campany *et al.*, (2016) observed for leaf g_m, mean whole-tree g_m did not differ between ambient and warmed trees (Fig. 3, Table S2), but there were some campaign-specific differences between temperature treatments ($P < 0.001$ for the campaign × warming interaction). Whole-tree g_m was higher in ambient than warmed trees in the summer (January; Fig. 2). The effects of the drought treatment varied across

campaigns (Table S2). Mean whole-tree g_m was marginally lower in droughted than in control trees ($P = 0.051$, Fig. 2) and there were some campaign-specific differences ($P < 0.001$ for the campaign × drought interaction) that also varied between temperature treatments ($P < 0.001$, for the campaign × warming × drought interaction). In March, whole-tree g_m was lower in droughted trees and this reduction was more pronounced in the warmed treatment (Fig. 2).

Overall, the response of whole-tree g_m (droughted trees excluded and only midday values under high light) to air temperature (T_{air}) was flat, but whole-tree g_m also showed complex non-linear trends that varied between ambient and warmed trees (Fig. 4). Between 25 and 30˚C, whole-tree g_m appeared to increase with T_{air}, in ambient trees, but not in trees experiencing warmer temperatures (Fig. 4). Beyond 35˚C (measured only in the mid-summer campaign in January), whole-tree g_m decreased with T_{air} in warmed trees (Fig. 4).

Seasonal patterns of $\delta^{13}C$ of photosynthesis and phloem contents

Both $\delta^{13}C$ of phloem contents ($\delta^{13}C_{ph}$) and of photosynthesis ($\delta^{13}C_{Anet}$) varied among campaigns but in an asynchronous manner (Fig. 5 and S4, Table S2). Warming had no significant effects on either $\delta^{13}C_{ph}$ or $\delta^{13}C_{Anet}$ whereas both $\delta^{13}C_{ph}$ and $\delta^{13}C_{Anet}$ were more enriched in droughted than in control trees (Table S2, Fig. S4). There was a significant linear relationship between $\delta^{13}C_{ph}$ and $\delta^{13}C_{Anet}$ (Table 1), but $\delta^{13}C_{ph}$ was consistently more depleted than $\delta^{13}C_{Anet}$ ($t = 9.4$, $P < 0.001$, Fig. 5). Measurements from the October, February and March campaigns fell along a line with a slope not significantly different from 1 (Table 1). In contrast, $\delta^{13}C_{ph}$ and $\delta^{13}C_{Anet}$ from the midsummer campaigns (December and January) showed a much larger spread and were not significantly correlated. Indeed, the relationship between $\delta^{13}C_{ph}$ and $\delta^{13}C_{Anet}$ became stronger (R^2_c increased from 0.14 to 0.7) when the data from the midsummer campaigns (December and January) were excluded (Table 1, Fig. 5).

Relationships between iWUE estimates and post-photosynthetic fractionation

The relationship between iWUE from gas-exchange ($iWUE_{ge}$, Eq. 1) and iWUE from $\delta^{13}C_{ph}$ was not significant when iWUE was calculated with the simplest discrimination model ($iWUE_{\Delta}$, Eq. 6, Fig. 6a, Table 1), which does not incorporate the effect of variable g_m on ^{13}C-discrimination. In contrast, there was a significant linear relationship between $iWUE_{ge}$ and iWUE calculated from a discrimination model incorporating the effect of g_m ($iWUE_{\Delta\text{-}gm}$, Eq. 8, Fig. 6b, Table1).

Furthermore, the slope of the relationship between mean (of each campaign and temperature treatment) $iWUE_{ge}$ and $iWUE_{\Delta\text{-}gm}$ was not significantly different from the 1:1 line (Fig. 7, slope±se: 0.96±0.27).

Finally, we estimated overall mean (±se, $n = 6$ campaigns) post-photosynthetic fractionation (Eq. 9) as 2.5 ± 0.7 ‰. We used this value of post-photosynthetic fractionation to recalculate $iWUE_{\Delta\text{-}gm\text{-}post}$ with $\delta^{13}C_{ph\text{-}corr}$ ($\delta^{13}C_{ph\text{-}corr} = \delta^{13}C_{ph} + 2.5$ ‰). When we incorporated this post-photosynthetic fractionation correction, we found that the intercept of the regression relationship between $iWUE_{ge}$ and $iWUE_{\Delta\text{-}gm\text{-}post}$ did not differ from zero and the slope was not different from 1:1 (Table 1, Fig. 7).

DISCUSSION

For the first time, we calculated whole-tree mesophyll conductance (g_m) over whole tall trees that reached 9 m in height at the end of the study. Whole-tree g_m values were similar to estimates derived from leaf cuvettes on the same trees. Warming had little direct effect on g_m except at high temperatures, whereas drought induced a reduction in whole-tree g_m that was more pronounced in the summer. Our results show that carbon isotopic composition of phloem contents ($\delta^{13}C_{ph}$) is a good proxy of whole-tree intrinsic water-use efficiency (iWUE), provided that the effect of g_m on ^{13}C-discrimination is taken into account. The ^{13}C-discrimination values in phloem contents were correlated with whole-tree photosynthetic discrimination, but with a consistent offset, presumably due to post-photosynthetic fractionations.

Whole-tree mesophyll conductance (g_m)

Mesophyll conductance (g_m) had seldom been calculated at scales above the leaf level. Keenan *et al.* (2010a) estimated g_m at the ecosystem scale from eddy covariance measurements and Schaufele *et al.*, (2011) estimated g_m at the canopy level for a crop, from measurements of whole-canopy ^{13}C-discrimination. That said, we know of no previous estimates of g_m at the whole-tree level except for that of Ubierna & Marshall, (2011), which relied on leaf-cuvette measurements to infer crown gas-exchange. Our estimates of whole-tree g_m were comparable to independent g_m estimates from leaf cuvette measurements averaged across both sun and shade leaves. This confirms that

whole-tree g_m integrated the entire crown, including the contrasting light sensitivities of g_m of sun and shade leaves (Campany *et al.*, 2016).

The calculation of g_m requires values for several parameters that are most often taken from the literature or from published relationships as a function of other variables, such as temperature. In our case, we benefited from concurrent studies at the same experimental site (Drake *et al.*, 2016; Drake *et al.*, 2019b), which meant we did not have to assume fixed values for such parameters. These included respiration (Aspinwall *et al.*, 2016) and the temperature-sensitivity of photorespiration (Way *et al.*, 2019), measured independently in the same experiment. The respiratory fractionation (e) was calculated as the mean difference between the $\delta^{13}C$ of CO_2 respired, obtained from measurements of WTC isotope exchange at night, and that of the respiratory substrates, assumed to be represented by the $\delta^{13}C_{ph}$ (Barbour *et al.*, 2007). With this approach, we calculated e = 3.4‰, which is well within the bounds of previous estimations (Barbour *et al.*, 2007; Wingate *et al.*, 2007). Measurements of e in the literature are scarce and, given that this parameter is likely to vary among species, with climatic and growth conditions (Dubbert *et al.*, 2012), it is desirable that studies like ours calculate and report that said value.

The response of whole-tree g_m to warming and drought across seasons agreed with previous findings from leaf-level measurements. Warming did not have a direct effect on whole-tree g_m, similar to findings with leaf g_m measured in the same experiment (Campany *et al.*, 2016). However, the warming treatment modified the temperature response of whole-tree g_m. Whole-tree g_m increased with temperature between 25 and 30˚C in trees that experienced ambient temperature, consistent with leaf-level observations from other *Eucalyptus* species (Warren, 2008a; von Caemmerer & Evans, 2015), but did not increase in the warmed trees. Furthermore, beyond 35˚C, whole-tree g_m decreased with temperature in warmed trees, consistent with previous observations for leaf g_m (Silim *et al.*, 2010). In our experiment, warming decreased both leaf respiration and photosynthesis to a similar extent (Aspinwall *et al.*, 2016). Hence, the observed response of whole-tree g_m to temperature is consistent with a coordinated response to warming of biochemical and diffusional limitations to photosynthesis, including g_m (Warren, 2008a; Grassi *et al.*, 2009).

Previous measurements of leaf g_m on *Eucalyptus* showed that leaf g_m decreases with water stress (Warren, 2008b; Cano *et al.*, 2014). Our whole-tree results agreed with these observations: we found lower whole-tree g_m in droughted trees in late summer (March), while these differences were reduced later in the season in autumn (April), when leaf water potential of droughted trees

418 partially recovered (Fig. S1). Temperature or drought sensitivities of physiological processes,
419 including g_m, can vary among crown layers (Cano *et al.*, 2013). Nonetheless, our results indicate
420 that overall, drought induced a reduction of crown-integrated g_m that was amplified under warmer
421 conditions.
422
423 *Phloem $\delta^{13}C$ combined with g_m provides a proxy for whole-tree iWUE*
424 The correlation between whole-tree iWUE estimates supports the use of $\delta^{13}C_{ph}$ as a proxy for
425 whole-tree iWUE, provided that g_m is accounted for in the calculations. Both $iWUE_{ge}$ (iWUE from
426 gas-exchange) and $iWUE_{\Delta\text{-}gm}$ (iWUE from $\delta^{13}C_{ph}$ incorporating the effect of g_m) were comparable
427 to measurements on the same species in a native woodland (Gimeno *et al.*, 2016, mean $iWUE_{ge}$:
428 78 μmol mol^{-1}). In our study, accounting for whole-tree g_m variation was sufficient to reconcile
429 estimates of iWUE from gas-exchange and C-isotopes. However, we note that there are other
430 factors that are not incorporated in the Δ_{gm} model (Eq. 7) that could result in biases under different
431 conditions. These factors are ternary effects, respiratory and photorespiratory fractionations. A
432 recent study by Ma *et al.*, (2020) demonstrated that the ternary effect on $iWUE_{\Delta}$ was small (~1%
433 error). Our measurements for iWUE analyses occurred when light intensity was above
434 800 μmol mol^{-1} and under these conditions, whole-tree ^{13}C-discrimination would have been
435 largely dominated by photosynthesis (Drake *et al.*, 2016). The contribution of photorespiration to
436 total discrimination is ~1‰ and varies with temperature; therefore, including this effect in
437 calculations of $iWUE_{\Delta}$ can improve predictions under some conditions (Ubierna & Farquhar,
438 2014). When choosing a $\Delta^{13}C$ model to derive $iWUE_{\Delta}$, one needs to consider the tradeoff between
439 complexity and goodness of fit. In our experiment, using the most simplified $\Delta^{13}C$ model (Eq. 5)
440 failed to capture physiological variability. The intermediate model including g_m (Eq. 7) did better,
441 but using the complete $\Delta^{13}C$ model did not further improve predictions of iWUE (Table S3).
442 Accordingly, the intermediate model was deemed a suitable compromise, as demonstrated by the
443 good agreement between $iWUE_{\Delta\text{-}gm}$ and $iWUE_{ge}$.
444 Calculations of $iWUE_{\Delta\text{-}gm}$ require values of g_m, which are often lacking from studies in
445 field settings and large trees. Whole-tree g_m was comparable to leaf g_m, a variable that has been
446 characterized for many species and plant functional types (Flexas *et al.*, 2012; Flexas *et al.*, 2014).
447 Additionally, there are eddy flux covariance sites where g_m has been measured independently (e.g.
448 Kooijmans *et al.*, 2019 or Gentsch *et al.*, 2014), and where $iWUE_{\Delta\text{-}gm}$ using $\delta^{13}C_{ph}$ can provide

449 independent validation of iWUE estimates from eddy covariance (Scartazza *et al.*, 2014).
450 Measuring whole-tree $iWUE_{ge}$ is technically challenging, whereas field sampling of $\delta^{13}C_{ph}$ is
451 comparatively easy and cost-effective. A caveat of this approach is that g_m is variable and its
452 variation is still poorly understood, despite modelling efforts (Sun *et al.*, 2014). Undoubtedly,
453 including a fixed value of g_m is better than including none, though our study showed that
454 accounting for variation in g_m was required for reconciling iWUE from gas-exchange and from
455 $\delta^{13}C_{ph}$. A systematic characterization of the response of g_m to environmental variation is necessary
456 to refine this approach.

457 Our experimental design allowed for a coarse characterization of post-photosynthetic
458 fractionation, estimated as 2.5‰ from the difference between $\delta^{13}C$ of photosynthesis ($\delta^{13}C_{Anet}$) and
459 $\delta^{13}C_{ph}$. The correlation between $iWUE_{ge}$ and $iWUE_{\Delta\text{-}gm}$ improved and became no different than
460 the 1:1 line when this offset was incorporated into our calculations. This 2.5‰ is consistent
461 previous estimates (Badeck *et al.*, 2005) and with the observations of Gessler *et al.*, (2007) for
462 *Eucalyptus delegatensis* at the base of the trunk, where diel oscillation of $\delta^{13}C_{ph}$ was most
463 attenuated. The dynamics of post-photosynthetic fractionation are not yet fully understood, and
464 even less so for tall trees, where phloem path lengths could further influence this process (Cernusak
465 *et al.*, 2009; Gessler *et al.*, 2014). Still, it appears that sampling of $\delta^{13}C_{ph}$ at the base of the tree
466 could represent the full crown, as modified by post-photosynthetic fractionation.

467 Differences in the temporal and spatial integration of photosynthate in the phloem could
468 also account for some of the offset between $\delta^{13}C_{Anet}$ and $\delta^{13}C_{ph}$. While the $\delta^{13}C_{Anet}$ was calculated
469 when photosynthesis peaked each day, the imprint of physiological processes on $\delta^{13}C_{ph}$ is likely
470 to reflect a longer time window, spanning several days (Keitel *et al.*, 2006; Powers & Marshall,
471 2011; Drake *et al.*, 2019a; Furze *et al.*, 2019). The $\delta^{13}C_{ph}$ was collected at one time of day and at
472 one point per tree (at a fixed location near the base of the bole). Our low sampling intensity could
473 have obscured potential variation in $\delta^{13}C_{ph}$ during the course of the day (Gessler *et al.*, 2007) or
474 with height along the trunk (e.g. Bogelein *et al.*, 2019). Still, our sampling protocol likely captured
475 the actual variability in $\delta^{13}C_{ph}$ that would have had an imprint on monthly whole-tree $iWUE_{\Delta}$. We
476 argue so, first, because $\delta^{13}C_{ph}$ at the base of the crown has been shown to integrate the whole plant
477 signal of ^{13}C-discrimination in recently fixed carbon (Barbour *et al.*, 2007; Gessler *et al.*, 2008)
478 and second because our measurements of $\delta^{13}C_{ph}$ were significantly correlated with $\delta^{13}C_{Anet}$,
479 measured independently. Furthermore, we found that $\delta^{13}C_{ph}$ under drought was enriched compared

to values for control trees, consistent with theory (Farquhar *et al.*, 1989; Cernusak *et al.*, 2003). On the other hand, the fact that $\delta^{13}C_{ph}$, but not $iWUE_{ge}$, responded to drought could suggest that under drought, $\delta^{13}C_{ph}$ could overestimate iWUE (Smith *et al.*, 2016). This would be especially critical if drought-induced variations in g_m were not taken into account.

Conclusions and future research avenues

Our results suggest that incorporating g_m into the calculations of $iWUE_{\Delta}$ could provide more reliable integrative estimates of whole-tree iWUE, reflecting the true impact of abiotic stress on vegetation-atmosphere carbon and water fluxes. Correcting for g_m is likely to reconcile iWUE estimates from gas-exchange and from $\delta^{13}C$, not only of the phloem, but of any plant material. In our study, leaf and whole-tree estimates of g_m were comparable and, fortunately, g_m has been extensively characterized for numerous species and plant functional types in the past few decades, mainly at the leaf-level (Flexas *et al.*, 2012; Flexas *et al.*, 2014). We suggest that field sampling of $\delta^{13}C_{ph}$, collected at the base of the crown, could be used to expand our current database of iWUE estimates worldwide (Cornwell *et al.*, 2017), including remote forests. However, further testing of the timing and sampling position would be crucial to compile a multi-species database of $iWUE_{\Delta}$, across biomes. Field sampling of $\delta^{13}C_{ph}$ across sites dominated by species for which WUE and g_m have been characterized would be the first step to explore the potential of this approach and then compile forest WUE estimates. Expanding the global network of WUE estimates should help constrain projections of carbon and water fluxes between forests and the atmosphere under future climate scenarios.

ACKNOWLEDGMENTS

We thank the editor (Dr Nate McDowell) and three anonymous referees for their comments. Thanks to Burhan Amiji for maintaining the WTC experiment and his outstanding technical assistance, to Claudia Keitel for her assistance during isotopic analyses and to Remko Duursma for his support during the design and experimental phases. We thank Sune Linder and the Swedish Agricultural University for providing the WTC. This study was supported by the Hawkesbury Institute for the Environment and Western Sydney University funds awarded to CEC and JDM. The WTC experiment was supported by a grant from the Australian Research Council

(DP140103415) awarded to MGT and JED. JDM was supported by KA Wallenberg Foundation (#2015.0047) during writing. TEG was supported by the Spanish Ministry of Science (Grant PHLISCO, PID2019-107817RB-I00).

AUTHOR CONTRIBUTIONS

CEC and JDM conceived and designed the study. MGT led the experimental design of the whole-tree chamber experiment. CEC measured online isotopic discrimination; collected, processed and analyzed all phloem samples. JED and CVMB collected and processed the gas-exchange measurements from the whole-tree chamber system. NU provided the theoretical framework for analyzing isotopic discrimination data. TEG and CEC analyzed the data. TEG wrote the first manuscript draft with significant input from JDM. All authors contributed to the writing.

REFERENCES

Aranda I, Forner A, Cuesta B, Valladares F. 2012. Species-specific water use by forest tree species: From the tree to the stand. *Agricultural Water Management* **114**: 67-77.

Aranda I, Pardos M, Puertolas J, Jimenez MD, Pardos JA. 2007. Water-use efficiency in cork oak (*Quercus suber*) is modified by the interaction of water and light availabilities. *Tree Physiology* **27**(5): 671-677.

Aspinwall MJ, Drake JE, Campany C, Varhammar A, Ghannoum O, Tissue DT, Reich PB, Tjoelker MG. 2016. Convergent acclimation of leaf photosynthesis and respiration to prevailing ambient temperatures under current and warmer climates in *Eucalyptus tereticornis*. *New Phytologist* **212**(2): 354-367.

Badeck FW, Tcherkez G, Nogues S, Piel C, Ghashghaie J. 2005. Post-photo synthetic fractionation of stable carbon isotopes between plant organs - a widespread phenomenon. *Rapid Communications in Mass Spectrometry* **19**(11): 1381-1391.

Barbour MM, Evans JR, Simonin KA, von Caemmerer S. 2016. Online CO_2 and H_2O oxygen isotope fractionation allows estimation of mesophyll conductance in C_4 plants, and reveals that mesophyll conductance decreases as leaves age in both C_4 and C_3 plants. *New Phytologist* **210**(3): 875-889.

Barbour MM, McDowell NG, Tcherkez G, Bickford CP, Hanson DT. 2007. A new measurement technique reveals rapid post-illumination changes in the carbon isotope composition of leaf-respired CO_2. *Plant, Cell and Environment* **30**(4): 469-482.

Barton CVM, Ellsworth DS, Medlyn BE, Duursma RA, Tissue DT, Adams MA, Eamus D, Conroy JP, McMurtrie RE, Parsby J, et al. 2010. Whole-tree chambers for elevated atmospheric CO_2 experimentation and tree scale flux measurements in south-eastern Australia: The Hawkesbury Forest Experiment. *Agricultural and Forest Meteorology* **150**(7-8): 941-951.

Bates D, Mächler M, Bolker B, Walker S. 2015. Fitting Linear Mixed-Effects Models Using lme4. *Journal of Statistical Software* **67**(1): 48.

Bogelein R, Lehmann MM, Thomas FM. 2019. Differences in carbon isotope leaf-to-phloem fractionation and mixing patterns along a vertical gradient in mature European beech and Douglas fir. *New Phytologist* **222**(4): 1803-1815.

Bowling DR, Ballantyne AP, Miller JB, Burns SP, Conway TJ, Menzer O, Stephens BB, Vaughn BH. 2014. Ecological processes dominate the ^{13}C land disequilibrium in a Rocky Mountain subalpine forest. *Global Biogeochemical Cycles* **28**(4): 352-370.

Busch FA, Holloway-Phillips M, Stuart-Williams H, Farquhar GD. 2020. Revisiting carbon isotope discrimination in C_3 plants shows respiration rules when photosynthesis is low. *Nature Plants* **6**(3): 245-258.

Campany CE, Tjoelker MG, von Caemmerer S, Duursma RA. 2016. Coupled response of stomatal and mesophyll conductance to light enhances photosynthesis of shade leaves under sunflecks. *Plant, Cell and Environment* **39**(12): 2762-2773.

Cano FJ, Lopez R, Warren CR. 2014. Implications of the mesophyll conductance to CO_2 for photosynthesis and water-use efficiency during long-term water stress and recovery in two contrasting *Eucalyptus* species. *Plant, Cell and Environment* **37**(11): 2470-2490.

Cano JF, Sanchez-Gomez D, Rodriguez-Calcerrada J, Warren CR, Gil L, Aranda I. 2013. Effects of drought on mesophyll conductance and photosynthetic limitations at different tree canopy layers. *Plant, Cell and Environment* **36**(11): 1961-1980.

Cernusak LA, Arthur DJ, Pate JS, Farquhar GD. 2003. Water relations link carbon and oxygen isotope discrimination to phloem sap sugar concentration in *Eucalyptus globulus*. *Plant Physiology* **131**(4): 1544-1554.

Cernusak LA, Tcherkez G, Keitel C, Cornwell WK, Santiago LS, Knohl A, Barbour MM, Williams DG, Reich PB, Ellsworth DS, et al. 2009. Viewpoint: Why are non-photosynthetic tissues generally ^{13}C enriched compared with leaves in C_3 plants? Review and synthesis of current hypotheses. *Functional Plant Biology* **36**(3): 199-213.

Cernusak LA, Ubierna N, Jenkins MW, Garrity SR, Rahn T, Powers HH, Hanson DT, Sevanto S, Wong SC, McDowell NG, Farquhar GD. 2018. Unsaturation of vapour pressure inside leaves of two conifer species. *Scientific Reports* **8**: 7667.

Cornwell WK, Wright IJ, Turner J, Maire V, Barbour MM, Cernusak L, Dawson T, Ellsworth DS, Farquhar GD, Griffiths H. 2017. A global dataset of leaf $\Delta^{13}C$ values. DOI: 10.5281/zenodo.569501

Dillaway DN, Kruger EL. 2010. Thermal acclimation of photosynthesis: a comparison of boreal and temperate tree species along a latitudinal transect. *Plant, Cell and Environment* **33**(6): 888-899.

Drake JE, Furze ME, Tjoelker MG, Carrillo Y, Barton CVM, Pendall E. 2019a. Climate warming and tree carbon use efficiency in a whole-tree (CO_2)-^{13}C tracer study. *New Phytologist* **222**(3): 1313-1324.

Drake JE, Tjoelker MG, Aspinwall MJ, Reich PB, Barton CVM, Medlyn BE, Duursma RA. 2016. Does physiological acclimation to climate warming stabilize the ratio of canopy respiration to photosynthesis? *New Phytologist* **211**(3): 850-863.

Drake JE, Tjoelker MG, Aspinwall MJ, Reich PB, Pfautsch S, Barton CVM. 2019b. The partitioning of gross primary production for young *Eucalyptus tereticornis* trees under experimental warming and altered water availability. *New Phytologist* **222**(3): 1298-1312.

Dubbert M, Rascher KG, Werner C. 2012. Species-specific differences in temporal and spatial variation in delta C-13 of plant carbon pools and dark-respired CO_2 under changing environmental conditions. *Photosynthesis Research* **113**(1-3): 297-309.

Duursma RA, Barton CVM, Lin YS, Medlyn BE, Eamus D, Tissue DT, Ellsworth DS, McMurtrie RE. 2014. The peaked response of transpiration rate to vapour pressure deficit in field conditions can be explained by the temperature optimum of photosynthesis. *Agricultural and Forest Meteorology* **189**: 2-10.

Duursma RA, Marshall JD. 2006. Vertical canopy gradients in delta $\delta^{13}C$ correspond with leaf nitrogen content in a mixed-species conifer forest. *Trees-Structure and Function* **20**(4): 496-506.

Eamus D. 1991. The interaction of rising CO_2 and temperatures with water-use efficiency. *Plant Cell, and Environment* **14**(8): 843-852.

Ehleringer JR, Field CB, Lin ZF, Kuo CY. 1986. Leaf carbon isotope and mineral-composition in subtropical plants along an irradiance cline. *Oecologia* **70**(4): 520-526.

Evans JR, Kaldenhoff R, Genty B, Terashima I. 2009. Resistances along the CO_2 diffusion pathway inside leaves. *Journal of Experimental Botany* **60**(8): 2235-2248.

Evans JR, Sharkey TD, Berry JA, Farquhar GD. 1986. Carbon isotope discrimination measured concurrently with gas-exchange to investigate CO_2 diffusion in leaves of higher-plants. *Australian Journal of Plant Physiology* **13**(2): 281-292.

Evans JR, von Caemmerer S. 2013. Temperature response of carbon isotope discrimination and mesophyll conductance in tobacco. *Plant Cell and Environment* **36**(4): 745-756.

Farquhar GD, Ball MC, von Caemmerer S, Roksandic Z. 1982. Effect of salinity and humidity on $\delta^{13}C$ value of halophytes-evidence for diffusional isotope fractionation determined by the ratio of intercellular/atmospheric partial pressure of CO_2 under different environmental conditions. *Oecologia* **52**(1): 121–124.

Farquhar G, Richards R. 1984. Isotopic Composition of Plant Carbon Correlates with Water-Use Efficiency of Wheat Genotypes. *Functional Plant Biology* **11**(6): 539-552.

Farquhar GD, Ehleringer JR, Hubick KT. 1989. Carbon isotope discrimination and photosynthesis. *Annual Review of Plant Physiology and Plant Molecular Biology* **40**: 503-537.

Flexas J, Barbour MM, Brendel O, Cabrera HM, Carriquí M, Díaz-Espejo A, Douthe C, Dreyer E, Ferrio JP, Gago J, et al. 2012. Mesophyll diffusion conductance to CO_2: An unappreciated central player in photosynthesis. *Plant Science* **193-194**: 70-84.

Flexas J, Carriqui M, Coopman RE, Gago J, Galmes J, Martorell S, Morales F, Diaz-Espejo A. 2014. Stomatal and mesophyll conductances to CO_2 in different plant groups: underrated factors for predicting leaf photosynthesis responses to climate change? *Plant Science* **226**: 41-48.

Flexas J, Diaz-Espejo A, Conesa MA, Coopman RE, Douthe C, Gago J, Galle A, Galmes J, Medrano H, Ribas-Carbo M, et al. 2016. Mesophyll conductance to CO_2 and Rubisco as targets for improving intrinsic water use efficiency in C_3 plants. *Plant, Cell and Environment* **39**(5): 965-982.

Fung I, Field CB, Berry JA, Thompson MV, Randerson JT, Malmstrom CM, Vitousek PM, Collatz GJ, Sellers PJ, Randall DA, et al. 1997. Carbon-13 exchanges between the atmosphere and biosphere. *Global Biogeochemical Cycles* **11**(4): 507-533.

Furze ME, Drake JE, Wiesenbauer J, Richter A, Pendall E. 2019. Carbon isotopic tracing of sugars throughout whole-trees exposed to climate warming. *Plant, Cell and Environment* **42**(12): 3253-3263.

Gentsch L, Hammerle A, Sturm P, Ogee J, Wingate L, Siegwolf R, Pluss P, Baur T, Buchmann N, Knohl A. 2014. Carbon isotope discrimination during branch photosynthesis of *Fagus sylvatica*: a Bayesian modelling approach. *Plant, Cell and Environment* **37**(7): 1516-1535.

Gessler A, Ferrio JP, Hommel R, Treydte K, Werner RA, Monson RK. 2014. Stable isotopes in tree rings: towards a mechanistic understanding of isotope fractionation and mixing processes from the leaves to the wood. *Tree Physiology* **34**(8): 796-818.

Gessler A, Keitel C, Kodama N, Weston C, Winters AJ, Keith H, Grice K, Leuning R, Farquhar GD. 2007. $\delta^{13}C$ of organic matter transported from the leaves to the roots in *Eucalyptus delegatensis*: short-term variations and relation to respired CO_2. *Functional Plant Biology* **34**(8): 692-706.

Gessler A, Tcherkez G, Peuke AD, Ghashghaie J, Farquhar GD. 2008. Experimental evidence for diel variations of the carbon isotope composition in leaf, stem and phloem sap organic matter in *Ricinus communis*. *Plant, Cell and Environment* **31**(7): 941-953.

Gimeno TE, Crous KY, Cooke J, O'Grady AP, Osvaldsson A, Medlyn BE, Ellsworth DS. 2016. Conserved stomatal behaviour under elevated CO_2 and varying water availability in a mature woodland. *Functional Ecology* **30**(5): 700-709.

Gimeno TE, Escudero A, Delgado A, Valladares F. 2012. Previous Land Use Alters the Effect of Climate Change and Facilitation on Expanding Woodlands of Spanish Juniper. *Ecosystems* **15**(4): 564-579.

Grassi G, Magnani F. 2005. Stomatal, mesophyll conductance and biochemical limitations to photosynthesis as affected by drought and leaf ontogeny in ash and oak trees. *Plant, Cell and Environment* **28**(7): 834-849.

Grassi G, Ripullone F, Borghetti M, Raddi S, Magnani F. 2009. Contribution of diffusional and non-diffusional limitations to midday depression of photosynthesis in *Arbutus unedo* L. *Trees-Structure and Function* **23**(6): 1149-1161.

Guerrieri R, Belmecheri S, Ollinger SV, Asbjornsen H, Jennings K, Xiao JF, Stocker BD, Martin M, Hollinger DY, Bracho-Garrillo R, et al. 2019. Disentangling the role of photosynthesis and stomatal conductance on rising forest water-use efficiency. *Proceedings of the National Academy of Sciences of the United States of America* **116**(34): 16909-16914.

Hsiao TC, Acevedo E. 1974. Plant responses to water deficits, water-use efficiency, and drought resistance. *Agricultural Meteorology* **14**(1-2): 59-84.

Keenan T, Sabate S, Gracia C. 2010a. The importance of mesophyll conductance in regulating forest ecosystem productivity during drought periods. *Global Change Biology* **16**(3): 1019-1034.

Keenan T, Sabate S, Gracia C. 2010b. Soil water stress and coupled photosynthesis-conductance models: Bridging the gap between conflicting reports on the relative roles of stomatal, mesophyll conductance and biochemical limitations to photosynthesis. *Agricultural and Forest Meteorology* **150**(3): 443-453.

Keenan TF, Hollinger DY, Bohrer G, Dragoni D, Munger JW, Schmid HP, Richardson AD. 2013. Increase in forest water-use efficiency as atmospheric carbon dioxide concentrations rise. *Nature* **499**(7458): 324-327.

Keitel C, Matzarakis A, Rennenberg H, Gessler A. 2006. Carbon isotopic composition and oxygen isotopic enrichment in phloem and total leaf organic matter of European beech (*Fagus sylvatica* L.) along a climate gradient. *Plant, Cell and Environment* **29**(8): 1492-1507.

Kohn MJ. 2010. Carbon isotope compositions of terrestrial C_3 plants as indicators of (paleo)ecology and (paleo)climate. *Proceedings of The National Academy of Sciences of the United States of America* **107**(46): 19691-19695.

Kooijmans LMJ, Sun W, Aalto J, Erkkila KM, Maseyk K, Seibt U, Vesala T, Mammarella I, Chen HL. 2019. Influences of light and humidity on carbonyl sulfide-based estimates of photosynthesis. *Proceedings of The National Academy of Sciences of the United States of America* **116**(7): 2470-2475.

Limousin JM, Misson L, Lavoir AV, Martin NK, Rambal S. 2010. Do photosynthetic limitations of evergreen *Quercus ilex* leaves change with long-term increased drought severity? *Plant, Cell and Environment* **33**(5): 863-875.

Ma WT, Tcherkez G, Wang XM, Schäufele R, Schnyder H, Yang Y, Gong XY. 2020. Revisiting the carbon isotope discrimination and water use efficiency relation: the influence of mesophyll conductance. bioRxiv preprint DOI: 10.1101/2020.07.06.188920.

Marshall JD, Linder S. 2013. Mineral nutrition and elevated CO_2 interact to modify $\delta^{13}C$, an index of gas exchange, in Norway spruce. *Tree Physiology* **33**(11): 1132-1144.

Marshall JD, Monserud RA. 1996. Homeostatic gas-exchange parameters inferred from $^{13}C/^{12}C$ in tree rings of conifers. *Oecologia* **105**(1): 13-21.

Maunoury F, Berveiller D, Lelarge C, Pontailler J-Y, Vanbostal L, Damesin C. 2006. Seasonal, daily and diurnal variations in the stable carbon isotope composition of carbon dioxide respired by tree trunks in a deciduous oak forest. *Oecologia* **151**(2): 268.

Medhurst J, Parsby J, Linder S, Wallin G, Ceschia E, Slaney M. 2006. A whole-tree chamber system for examining tree-level physiological responses of field-grown trees to environmental variation and climate change. *Plant, Cell and Environment* **29**(9): 1853-1869.

Medlyn BE, De Kauwe MG, Lin YS, Knauer J, Duursma RA, Williams CA, Arneth A, Clement R, Isaac P, Limousin JM, et al. 2017. How do leaf and ecosystem measures of water-use efficiency compare? *New Phytologist* **216**(3): 758-770.

Merchant A, Tausz M, Keitel C, Adams MA. 2010. Relations of sugar composition and delta ^{13}C in phloem sap to growth and physiological performance of *Eucalyptus globulus* (Labill). *Plant, Cell and Environment* **33**(8): 1361-1368.

Michelot A, Eglin T, Dufrêne E, Lelarge-Trouverie C, Damesin C. 2011. Comparison of seasonal variations in water-use efficiency calculated from the carbon isotope composition of tree rings and flux data in a temperate forest. *Plant, Cell and Environment* **34**(2): 230-244.

Nakagawa S, Schielzeth H. 2013. A general and simple method for obtaining R2 from generalized linear mixed-effects models. *Methods in Ecology and Evolution* **4**(2): 133-142.

Niinemets U, Diaz-Espejo A, Flexas J, Galmes J, Warren CR. 2009. Role of mesophyll diffusion conductance in constraining potential photosynthetic productivity in the field. *Journal of Experimental Botany* **60**(8): 2249-2270.

Pate J, Shedley E, Arthur D, Adams M. 1998. Spatial and temporal variations in phloem sap composition of plantation-grown *Eucalyptus globulus*. *Oecologia* **117**(3): 312-322.

Peters W, van der Velde IR, van Schaik E, Miller JB, Ciais P, Duarte HF, van der Laan-Luijkx IT, van der Molen MK, Scholze M, Schaefer K, et al. 2018. Increased water-use efficiency and reduced CO_2 uptake by plants during droughts at a continental scale. *Nature Geoscience* **11**(10): 744-748.

Pons TL, Flexas J, von Caemmerer S, Evans JR, Genty B, Ribas-Carbo M, Brugnoli E. 2009. Estimating mesophyll conductance to CO_2: methodology, potential errors, and recommendations. *Journal of Experimental Botany* **60**(8): 2217-2234.

Powers EM, Marshall JD. 2011. Pulse labeling of dissolved ^{13}C-carbonate into tree xylem: developing a new method to determine the fate of recently fixed photosynthate. *Rapid Communications in Mass Spectrometry* **25**(1): 33-40.

Qiu CP, Ethier G, Pepin S, Dube P, Desjardins Y, Gosselin A. 2017. Persistent negative temperature response of mesophyll conductance in red raspberry (*Rubus idaeus* L.) leaves under both high and low vapour pressure deficits: a role for abscisic acid? *Plant, Cell and Environment* **40**(9): 1940-1959.

R Development Core Team R. 2019. R: A Language and Environment for Statistical Computing. Vienna. Austria: R foundation for statistical computing.

Raczka B, Duarte HF, Koven CD, Ricciuto D, Thornton PE, Lin JC, Bowling DR. 2016. An observational constraint on stomatal function in forests: evaluating coupled carbon and water vapor exchange with carbon isotopes in the Community Land Model (CLM4.5). *Biogeosciences* **13**(18): 5183-5204.

Rogers A, Medlyn BE, Dukes JS, Bonan G, von Caemmerer S, Dietze MC, Kattge J, Leakey ADB, Mercado LM, Niinemets U, et al. 2017. A roadmap for improving the representation of photosynthesis in Earth system models. *New Phytologist* **213**(1): 22-42.

Scartazza A, Moscatello S, Matteucci G, Battistelli A, Brugnoli E. 2015. Combining stable isotope and carbohydrate analyses in phloem sap and fine roots to study seasonal changes of source-sink relationships in a Mediterranean beech forest. *Tree Physiology* **35**(8): 829-839.

Scartazza A, Vaccari FP, Bertolini T, Di Tommasi P, Lauteri M, Miglietta F, Brugnoli E. 2014. Comparing integrated stable isotope and eddy covariance estimates of water-use efficiency on a Mediterranean successional sequence. *Oecologia* **176**(2): 581-594.

Schaufele R, Santrucek J, Schnyder H. 2011. Dynamic changes of canopy-scale mesophyll conductance to CO_2 diffusion of sunflower as affected by CO_2 concentration and abscisic acid. *Plant, Cell and Environment* **34**(1): 127-136.

Seibt U, Rajabi A, Griffiths H, Berry JA. 2008. Carbon isotopes and water use efficiency: sense and sensitivity. *Oecologia* **155**(3): 441-454.

Sellers PJ, Dickinson RE, Randall DA, Betts AK, Hall FG, Berry JA, Collatz GJ, Denning AS, Mooney HA, Nobre CA, et al. 1997. Modeling the exchanges of energy, water, and carbon between continents and the atmosphere. *Science* **275**(5299): 502-509.**Shrestha A, Song X, Barbour MM. 2019.** The temperature response of mesophyll conductance, and its component conductances, varies between species and genotypes. *Photosynthesis Research* **141**(1): 65-82.

Silim SN, Ryan N, Kubien DS. 2010. Temperature responses of photosynthesis and respiration in *Populus balsamifera* L.: acclimation versus adaptation. *Photosynthesis Research* **104**(1): 19-30.

Smith M, Wild B, Richter A, Simonin K, Merchant A. 2016. Carbon Isotope Composition of Carbohydrates and Polyols in Leaf and Phloem Sap of *Phaseolus vulgaris* L. Influences Predictions of Plant Water Use Efficiency. *Plant and Cell Physiology* **57**(8): 1756-1766.

Sun Y, Gu LH, Dickinson RE, Norby RJ, Pallardy SG, Hoffman FM. 2014. Impact of mesophyll diffusion on estimated global land CO_2 fertilization. *Proceedings of The National Academy of Sciences of the United States of America* **111**(44): 15774-15779.

Tarin T, Nolan RH, Medlyn BE, Cleverly J, Eamus D. 2020. Water-use efficiency in a semi-arid woodland with high rainfall variability. *Global Change Biology* **26**(2): 496-508.

Théroux-Rancourt G, Gilbert ME. 2017. The light response of mesophyll conductance is controlled by structure across leaf profiles. *Plant, Cell and Environment* **40**(5): 726-740.

Tomas M, Flexas J, Copolovici L, Galmes J, Hallik L, Medrano H, Ribas-Carbo M, Tosens T, Vislap V, Niinemets U. 2013. Importance of leaf anatomy in determining mesophyll diffusion conductance to CO_2 across species: quantitative limitations and scaling up by models. *Journal of Experimental Botany* **64**(8): 2269-2281.

Ubierna N, Marshall JD. 2011. Estimation of canopy average mesophyll conductance using delta $\delta^{13}C$ of phloem contents. *Plant Cell and Environment* **34**(9): 1521-1535.

Ubierna N, Farquhar GD. 2014. Advances in measurements and models of photosynthetic carbon isotope discrimination in C_3 plants. *Plant Cell and Environment* **37**(7): 1494-1498.

Vernay A, Tian X, Chi J, Linder S, Mäkelä A, Oren R, Peichl M, Stangl ZR, Tor-Ngern P, Marshall JD. 2020. Estimating canopy gross primary production by combining phloem stable isotopes with canopy and mesophyll conductances. *Plant, Cell and Environment* **43**(9): 2124-2142.

Veromann-Jurgenson LL, Tosens T, Laanisto L, Niinemets U. 2017. Extremely thick cell walls and low mesophyll conductance: welcome to the world of ancient living! *Journal of Experimental Botany* **68**(7): 1639-1653.

von Caemmerer S, Evans JR. 2015. Temperature responses of mesophyll conductance differ greatly between species. *Plant, Cell and Environment* **38**(4): 629-637.

von Caemmerer S, Farquhar GD. 1981. Some relationships between the biochemistry of photosynthesis and the gas-exchange of leaves. *Planta* **153**(4): 376-387.

Warren CR. 2008a. Does growth temperature affect the temperature responses of photosynthesis and internal conductance to CO_2? A test with *Eucalyptus regnans*. *Tree Physiology* **28**(1): 11-19.

Warren CR. 2008b. Soil water deficits decrease the internal conductance to CO_2 transfer but atmospheric water deficits do not. *Journal of Experimental Botany* **59**(2): 327-334.

Warren CR, Dreyer E. 2006. Temperature response of photosynthesis and internal conductance to CO_2: results from two independent approaches. *Journal of Experimental Botany* **57**(12): 3057-3067.

Way DA, Aspinwall MJ, Drake JE, Crous KY, Campany CE, Ghannoum O, Tissue DT, Tjoelker MG. 2019. Responses of respiration in the light to warming in field-grown trees: a comparison of the thermal sensitivity of the Kok and Laisk methods. *New Phytologist* **222**(1): 132-143.

Wingate L, Seibt U, Moncrieff J, Lloyd J, Berry J. 2007. Variations in ^{13}C discrimination during CO_2 exchange in *Picea sitchensis* branches in the field. *Plant, Cell and Environment* **30**: 600-616.

SUPPORTING INFORMATION

The following Supporting Information is available for this article:

Table S1. Measurement campaign dates, whole-tree chambers measured and climatic conditions.

Table S2. Results of the linear mixed models for the effects of measurement campaign, warming and drought treatments and their interactions.

Table S3. Results of the regression relationships between C_i calculated from gas-exchange and from ^{13}C discrimination (Δ) using different assumptions.

Fig. S1. Soil volumetric water content and pre-dawn leaf water potential from the whole-tree chambers along the experiment.

Fig. S2. Sub-daily measurements of photosynthetic discrimination and physiological variables.

Fig. S3. Whole-tree stomatal conductance, photosynthesis, intrinsic water-use efficiency and phloem carbon isotopic composition.

Fig. S4. Boxplots of carbon isotope composition.

Methods S1. Calculations of whole-tree gas-exchange parameters and mesophyll conductance

Methods S2. Calculations of C_i from ^{13}C photosynthetic discrimination.

TABLES AND FIGURES

Table 1. Intercept and slope estimates (se) from the linear mixed models for the regression relationships between intrinsic water-use efficiency (iWUE in μmol mol^{-1}) and carbon isotopic composition ($\delta^{13}C$ in ‰) of the phloem contents ($\delta^{13}C_{ph}$) and of midday photosynthesis ($\delta^{13}C_{Anet}$). iWUE was calculated from measurements of gas-exchange ($iWUE_{ge}$) and from $\delta^{13}C_{ph}$ according to either Eq. 6 ($iWUE_{\Delta}$, simple ^{13}C discrimination model) or Eq. 8 ($iWUE_{\Delta\text{-}gm}$, discrimination model incorporating the effect of mesophyll conductance). $iWUE_{\Delta\text{-}gm\text{-}post}$ was calculated using $\delta^{13}C_{ph}$ corrected for estimated post-photosynthetic fractionation (2.5‰). Values significantly different from zero ($P < 0.05$) are indicated in **bold**. Marginal (R^2_m) or conditional (R^2_m) variance coefficients represent the variance explained by fixed or by both fixed and random factors, respectively.

Regression relationship		**Intercept**	**Slope**	$\boldsymbol{R^2_m}$	$\boldsymbol{R^2_c}$
$iWUE_{ge}$	$iWUE_{\Delta}$ (Eq. 6)	**65 (23)**	0.35 (0.25)	0.04	0.04
	$iWUE_{\Delta\text{-}gm}$ (Eq. 8)	**46 (13)**	**0.61 (0.16)**	0.23	0.23
	$iWUE_{\Delta\text{-}gm\text{-}post}$ (Eq. 6 & 9)	30 (17)	**0.61 (0.16)**	0.23	0.23
$\delta^{13}C_{ph}$	$\delta^{13}C_{Anet}$	**-23 (2.9)**	**0.26 (0.1)**	0.11	0.14
	$\delta^{13}C_{Anet}$†	-5.5 (2.9)	**0.85 (0.1)**	0.68	0.68

†Excluding data from the summer (December and January) campaigns.

FIGURE LEGENDS

Figure 1. Schematic representation of the theoretical model for calculating whole-tree intrinsic water-use efficiency (iWUE) from ^{13}C discrimination. Carbon isotope discrimination (Δ) is calculated from the difference in carbon isotopic composition between ambient air (δ_a) and that of the phloem contents (δ_{ph}). The model for Δ incorporates the effects of fractionation due to diffusion through the stomata (a_s), diffusion through the liquid phase (a_i) and carboxylation (b). iWUE is the ratio of photosynthesis (A_{net}) to stomatal conductance to water (g_s), calculated from transpiration (E) and vapor pressure defitic (D_w). CO_2 diffuses through the stomata (g_s) from the atmosphere (C_a) into the substomatal cavity (C_i) and finally through the mesophyll (g_m is the mesophyll conductance to CO_2) into the sites of carboxylation (C_c). Here A_{net}, E, D_w, g_s, C_a, C_i, g_m and δ_a were obtained from whole-tree chamber measurements of gas- and isotope-exchange. Note that the Δ equation is equivalent to Eq. 7.

Figure 2. Whole-tree mesophyll conductance (g_m) determined at midday under prevailing ambient conditions, spanning spring through autumn, in each treatment combination. Mean (+se, n = 6 trees for Oct-Jan and n = 3 for Feb-Apr, expect for Feb ambient control where n = 1) whole-tree g_m in *Eucalyptus tereticornis* in the six measurement campaigns in ambient (blue) and warmed (ambient +3°C, red) trees under control (solid bars) or drought (striped bars). Asterisks (*), crosses (+) and hashtags (#) indicate significant differences ($P < 0.05$) between temperature treatments within the control watering regime (*), and between control and drought trees within ambient (+) or warmed (#) trees.

Figure 3. Comparison of whole-tree and leaf mesophyll conductance (g_m). Mean (+se, n = 6 campaigns, drought trees excluded) whole-tree (measured in this study) and leaf g_m in *Eucalyptus tereticornis* from Campany *et al.*, (2016) in ambient (blue) and warmed (ambient + 3 °C, red) trees. There were no significant differences between temperature treatments.

Figure 4. Effect of air temperature (T_{air}) on midday whole-tree mesophyll conductance (g_m). Points are individual measurements of ln-transformed whole-tree g_m (in mmol mol^{-1}) in *Eucalyptus tereticornis* at varying T_{air} in ambient (blue) and warmed (ambient +3 °C, red) trees (drought trees

excluded). Different symbol shapes depict the six measurement campaigns. The lines are the smooth curves (fitted with a generalized additive mixed model) and the shaded polygons are the 95% confidence intervals.

Figure 5. Relationship between C isotopic composition of the bole phloem ($\delta^{13}C_{ph}$) and of midday whole-tree photosynthesis ($\delta^{13}C_{Anet}$) in *Eucalyptus tereticornis*. Symbol shapes depict measurement campaigns, colors depict ambient (blue) and warmed (ambient +3 °C, red) trees and closed and open symbols depict control and drought trees (only for February and March during the austral late summer), respectively. Large symbols with error bars are the means (±se, n = 6 trees) per campaign and temperature treatment with control and drought trees (for February and March) pooled for clarity. Smaller symbols without error bars are individual tree measurements. The dashed line is the 1:1 line and solid lines are the fitted linear relationships with either all measurements (grey) or excluding the summertime (December and January) data (black).

Figure 6. Correlations between intrinsic water use efficiency (iWUE) from different methods. Correlation between iWUE in *Eucalyptus tereticornis* calculated from whole-tree gas-exchange ($iWUE_{ge}$) and from carbon isotopic composition of the phloem calculated according to either **(a)** Eq. 6, simple ^{13}C-discrimination model ($iWUE_{\Delta}$), or **(b)** Eq. 8, discrimination model incorporating the effect of mesophyll conductance ($iWUE_{\Delta\text{-}gm}$). Large symbols with error bars are the means (±se, n = 6 trees) per campaign and temperature treatment with control and drought trees (for February and March) pooled for clarity. Smaller symbols without error bars are individual tree measurements. Symbol shapes depict measurement campaigns, colors depict ambient (blue) and warmed (ambient +3 °C, red) trees and closed and open symbols depict control and drought trees (only for February and March), respectively. Line in **(b)** is the linear fitted relationship to individual measurements. The linear relationship in **(a)** was not significant.

Figure 7. Effect of post-photosynthetic fractionation on the correlation between intrinsic water-use efficiency (iWUE) estimates. Correlation between mean (±se, n = 6 trees, control and drought trees for the February and March campaigns have been pooled) iWUE from gas-exchange ($iWUE_{ge}$) and from phloem contents C isotopic composition, corrected for post-photosynthetic fractionation and accounting for the effect of whole-tree mesophyll conductance ($iWUE_{\Delta\text{-}gm\text{-}post}$)

in *Eucalyptus tereticornis*. The solid line is the linear regression (P = 0.007, R^2 = 0.62) fitted to the mean values between $iWUE_{ge}$ and $iWUE_{\Delta\text{-}gm\text{-}post}$. The regression was not significantly different from the 1:1 dashed line (slope: 0.96 ± 0.27).

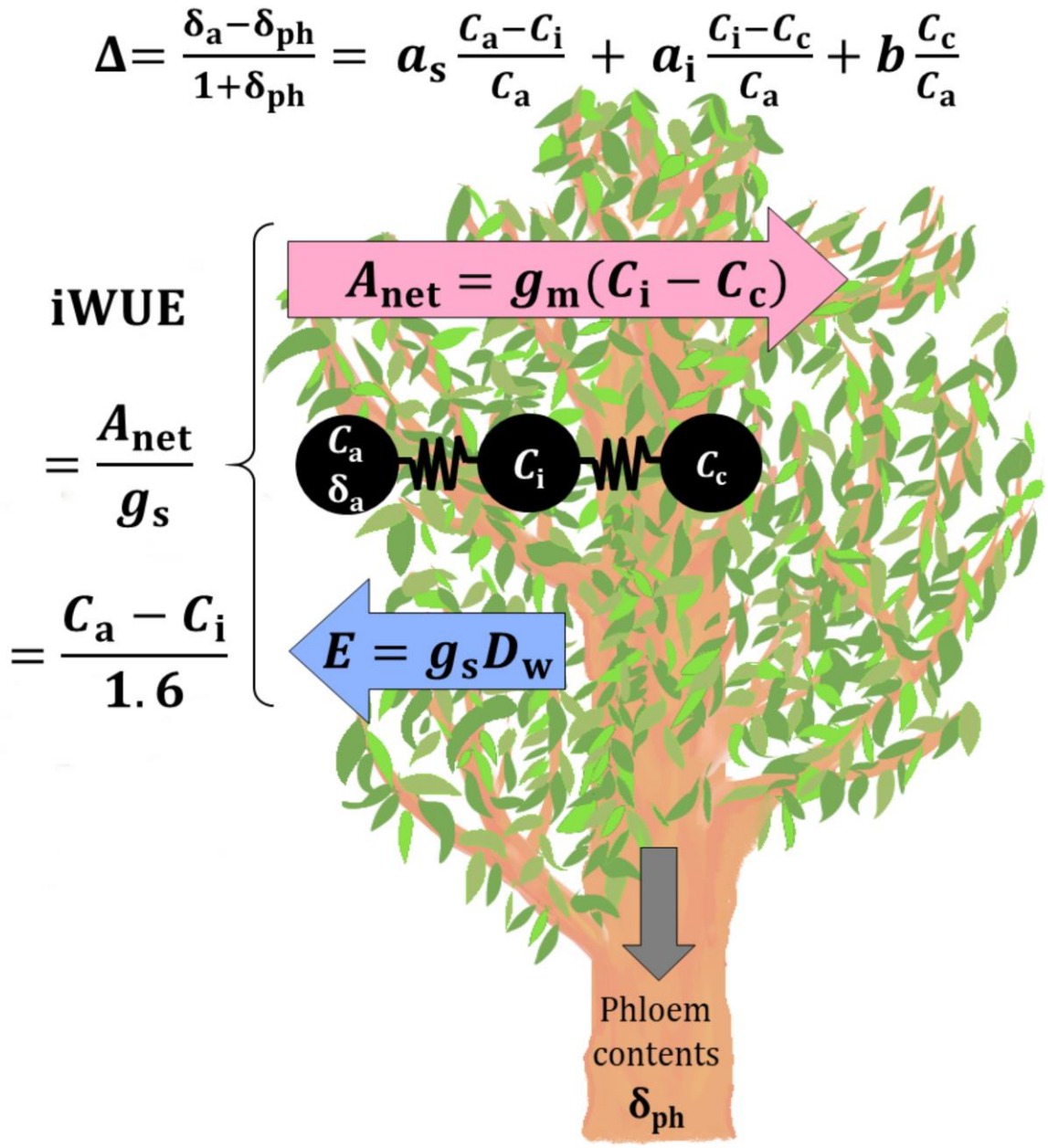

899

900 **Figure 1.**

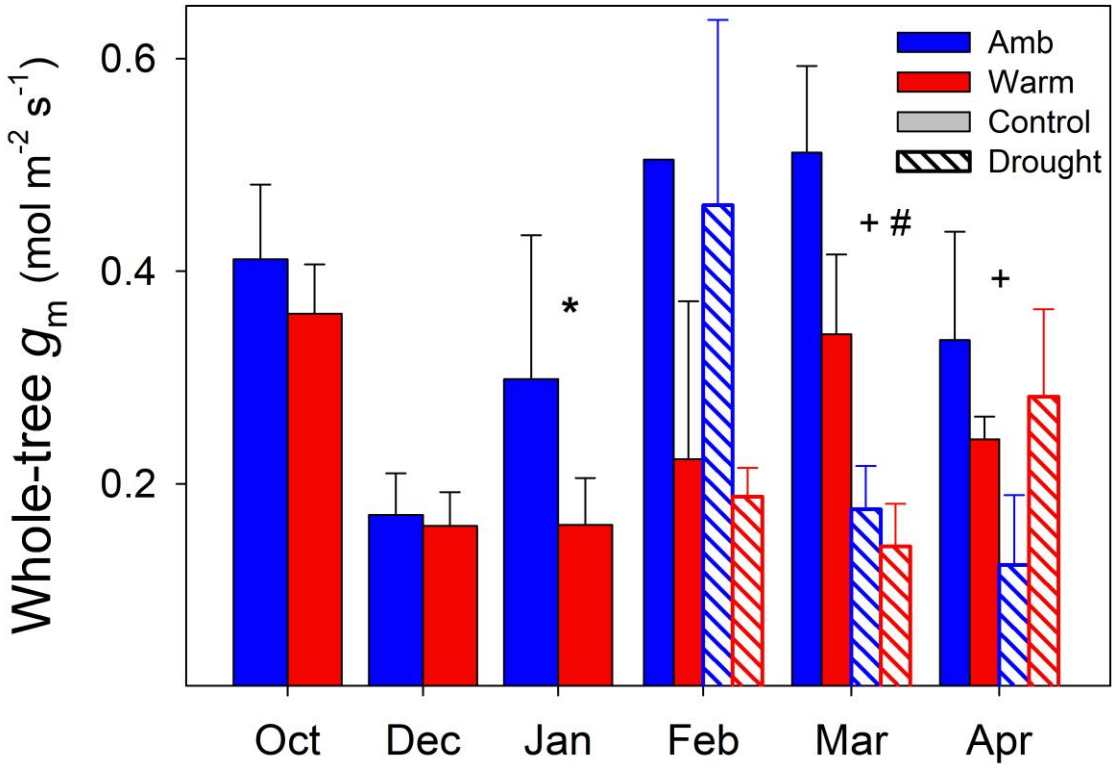

901

902 **Figure 2.**

903

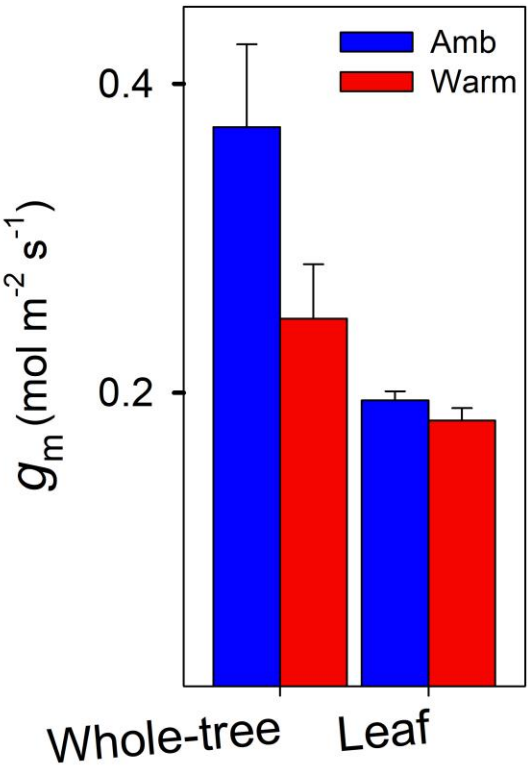

904

905 **Figure 3.**

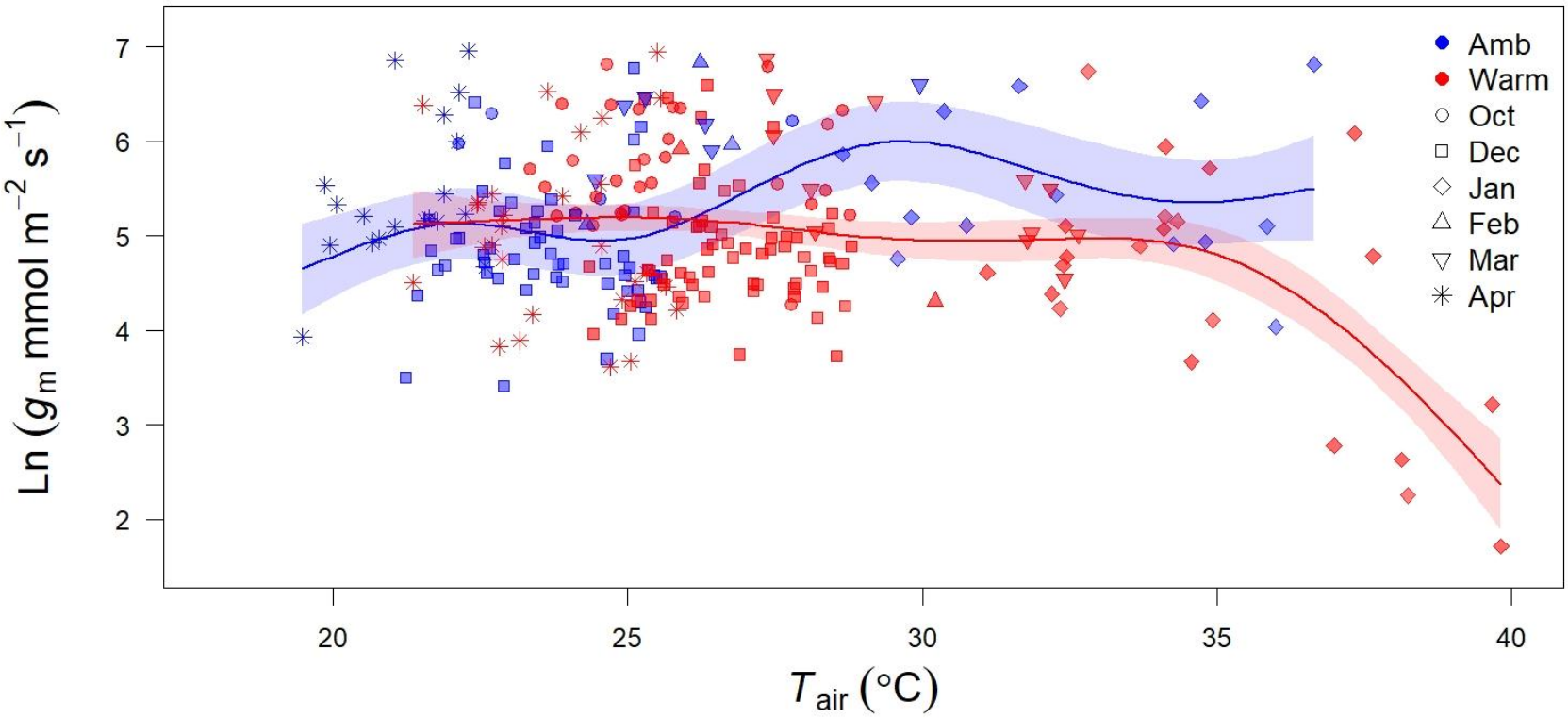

906

907 **Figure 4.**

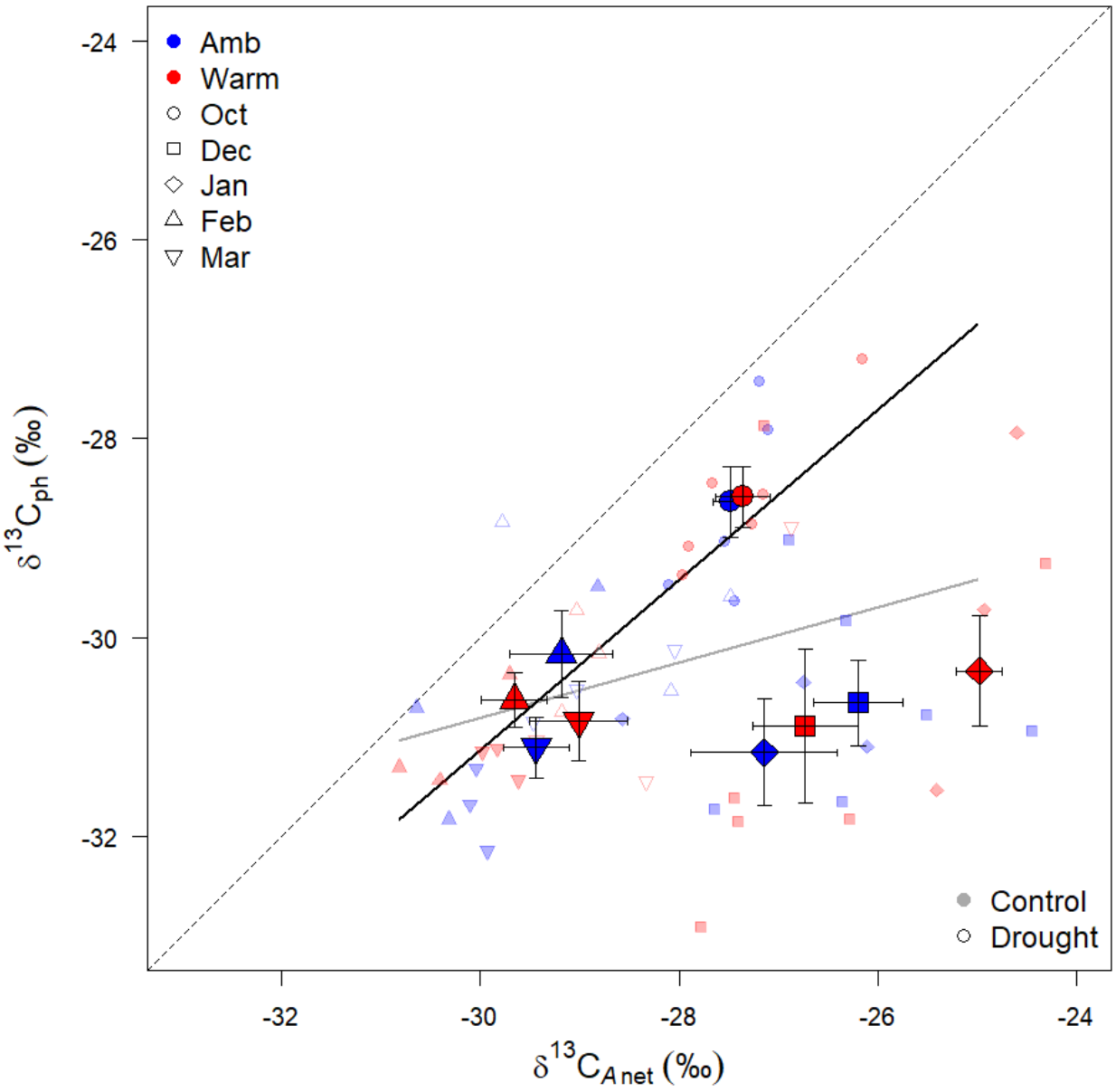

908

909 **Figure 5.**

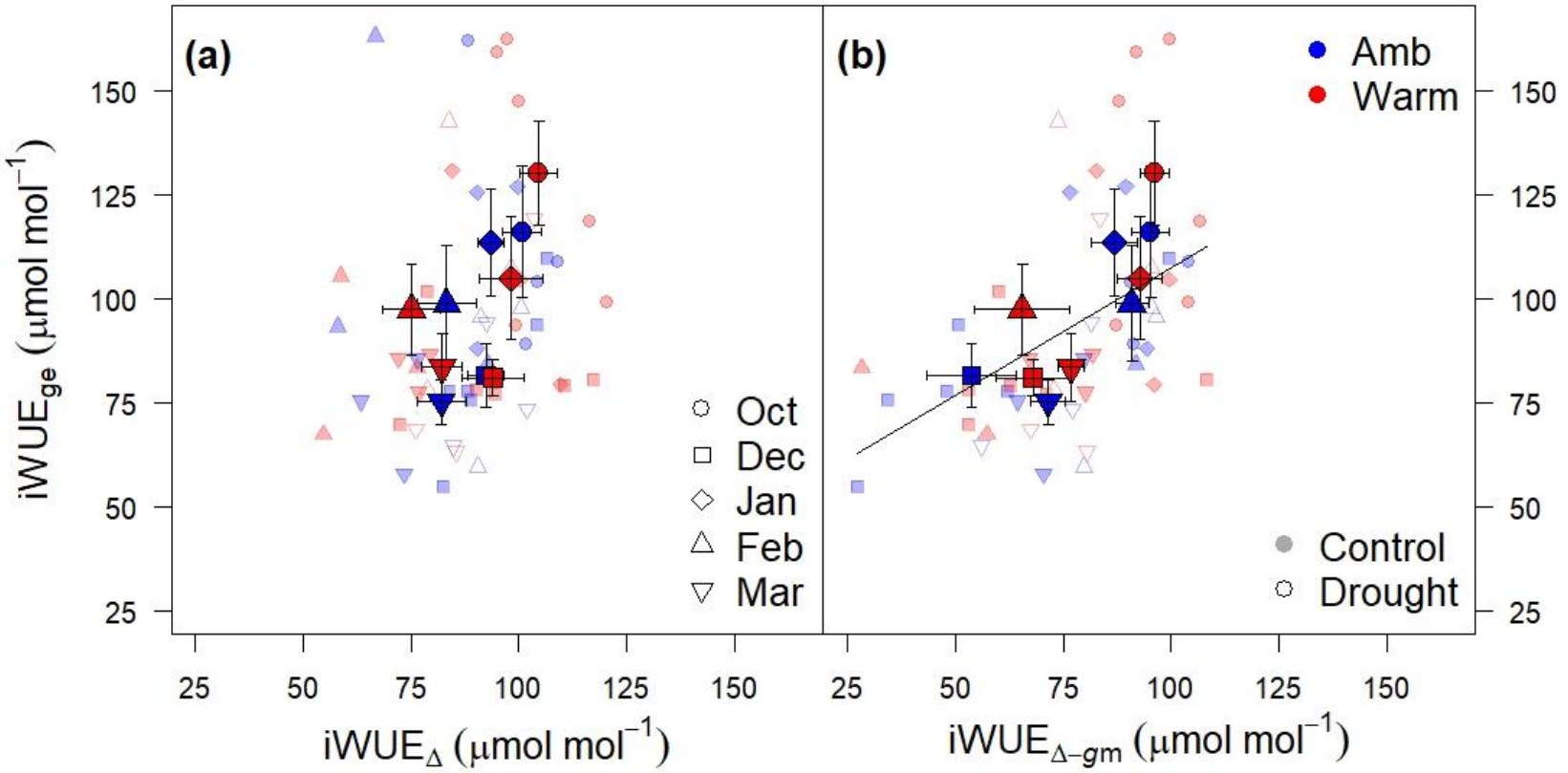

910

911 **Figure 6.**

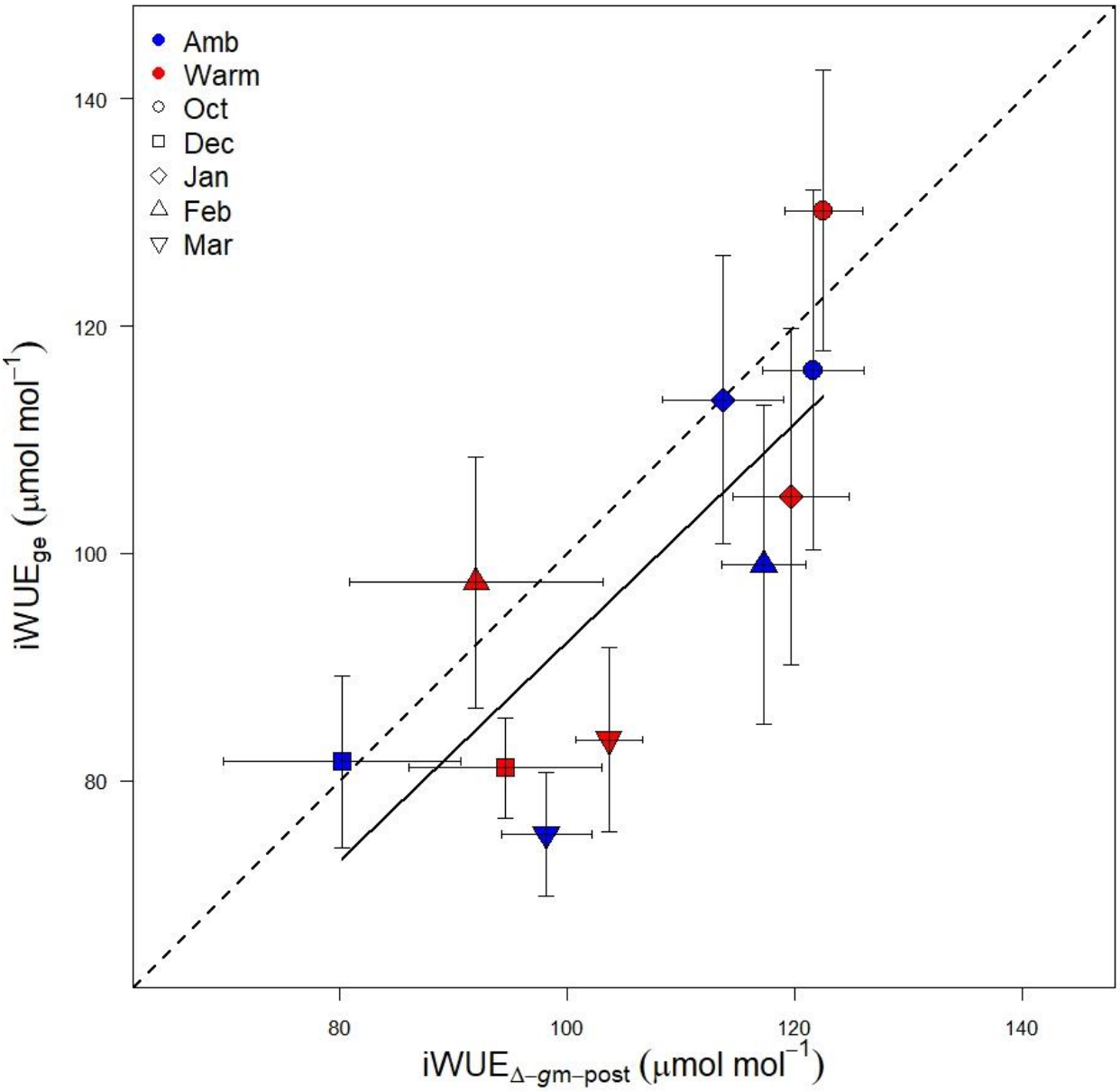

912

913 **Figure 7.**